

Contents lists available at ScienceDirect

Journal of the Mechanics and Physics of Solids

journal homepage: www.elsevier.com/locate/jmps





Experimental molecular dynamics for individual atomic-scale plastic events in nanoscale crystals

Sixue Zheng ^a, Shuhei Shinzato ^b, Shigenobu Ogata ^b, Scott X. Mao ^{a,*}

- ^a Department of Mechanical Engineering and Materials Science, University of Pittsburgh, Pittsburgh, PA 15261, USA
- ^b Department of Mechanical Science and Bioengineering, Osaka University, Osaka 560-8531, Japan

ARTICLE INFO

Keywords: Atomic scale Individual plastic events Stress-strain curves Nanoscale metals

ABSTRACT

The experimental determination of critical stresses for yielding and plastic flow is of upmost importance for the understanding of the atomic-scale mechanical behaviors of nanoscale metals, which is limited in computational molecular dynamics due to their inherent high strain rates and empirical interatomic potentials. Here, we propose an *in situ* atomic-scale experimental mechanics, the so-called experimental molecular dynamics, which is capable of studying the stress-strain relations with respect to the individual atomic-scale plastic events, including full dislocation slip, deformation twinning and shear band in nanoscale metals with different crystal structures. The local stress, strain and their relationships were obtained based on the analyses of the change in lattice strain gauge, interplanar spacing and gauge length. Using this method, drastic stress drops and strain bursts, the characteristics of individual plastic events, are investigated. The critical stresses for activating the nucleation and growth of atomic-scale defects are obtained. The newly developed experimental molecular dynamics with *in situ* mechanics approach has the advantage of quasi-static strain rate and no requirement of interatomic potentials over the computational one, which may provide new clues to establish the stress-based criteria for atomic-scale yielding and plastic flow.

1. Introduction

Nanoscale metals with superior physical and mechanical properties are envisioned as promising building blocks in stretchable electronic devices and flexible electronics (Cui et al., 2018; Liang et al., 2014; Rogers et al., 2010; Stoppa and Chiolerio, 2014; Xu and Zhu, 2012; Yin et al., 2019b). To guarantee the reliability and stability of nanoscale-metals-based devices, the determination of critical stress for activating individual atomic-scale plastic event in nanoscale metals, such as dislocation slip and deformation twinning, have recently stirred an upsurge in theoretical and experimental interests. Thus far, current knowledge on the atomic-scale deformation processes and the resultant stress-strain behaviors in nanostructured metals mostly relies on Molecular dynamics (MD) simulations. The computational methods, however, are limited by computational resources so that they are normally conducted at high strain rates (usually $10^7 - 10^9/s$) (Fan et al., 2012; Ramachandramoorthy et al., 2015b; Zhu et al., 2008). Furthermore, atomistic simulations also suffered from the approximate nature of empirical or semi-empirical interatomic potentials (Deng and Sansoz, 2009; Park et al., 2015; Zheng et al., 2010) and the uncertainty in the shape of nanoscale metals (Wang et al., 2013a). Due to these limitations, whether the atomistic simulation results can be directly extrapolated to those under laboratory conditions remains an open question. New

E-mail address: sxm2@pitt.edu (S.X. Mao).

^{*} Corresponding author.

experimental mechanics at the atomic scale, validating the discoveries from MD simulations, is thus in urgent need.

Newly developed transmission electron microscopy (TEM)-based *in situ* nanomechanical testing is capable of directly visualizing the atomic-scale and time-resolved deformation processes in nanoscale metals (Park et al., 2009; Wang and Mao, 2016; Wang et al., 2018d; Zheng and Mao, 2021; Zhu, 2017). Furthermore, the sample dimensions studied by *in situ* experimental mechanics are comparable to those used in MD simulations, allowing direct comparisons between the experimental and computational results. Recent experimental investigations on the atomic-scale deformation mechanisms in nanoscale metals, including length scale-dependent dislocation nucleation (Chen et al., 2015; Oh et al., 2009; Zheng et al., 2010), dislocation slip (Cao et al., 2018; Wang et al., 2018c), deformation twinning (He et al., 2020; Wang et al., 2015b), interface-related deformation (Wang et al., 2013b; Yin et al., 2020; Zhu et al., 2019), phase transformation (Lu et al., 2020; Zhang et al., 2021), surface diffusion-mediated deformation (Sun et al., 2019; Zhong et al., 2017) and reversible structure-transition-induced pseudoelasticity (Sun et al., 2014a; Wang et al., 2020b; Zheng et al., 2012), provided direct evidence to prove or disprove computational results. *In situ* experimental mechanics, however, failed to obtain one to one correspondence between atomic-scale deformation behaviors and stress-strain relations in nanoscale metals, which is technical demanding. A better understanding of the stress-strain behaviors with respect to the individual atomic-scale plastic events is becoming increasingly important for not only establishing a complete structure-property-deformation map of nanostructured metals but also realizing their potential applications in the next generation nanodevices.

In this article, we firstly propose an experimental method based on *in situ* atomic-scale experimental mechanics with high resolution transmission electron microscopy (HRTEM), that is called experimental molecular dynamics, which is capable of studying stress-strain responses with respect to the individual atomic-scale plastic events in nanoscale metals, based on the change in interplanar spacing along loading direction and the sample gauge length. Subsequently, we analyze and discuss the stress drops and strain bursts, caused by the individual plastic events, including full dislocation slip, deformation twinning and shear band in face-centered cubic (FCC), body-centered cubic (BCC) and hexagonal close-packed (HCP) nanocrystals. The critical stresses for activating the nucleation and growth of atomic-scale defects are obtained. Theoretical analyses, and the comparisons between experimental and computational results demonstrate that experimental molecular dynamics is feasible and effective. Finally, the prospect of future research about experimental molecular dynamics will be discussed.

2. Methods

2.1. Experimental molecular dynamics

As the nanoscale metals are expected to be widely used in the stretchable and flexible electronics (Cui et al., 2018; Liang et al.,

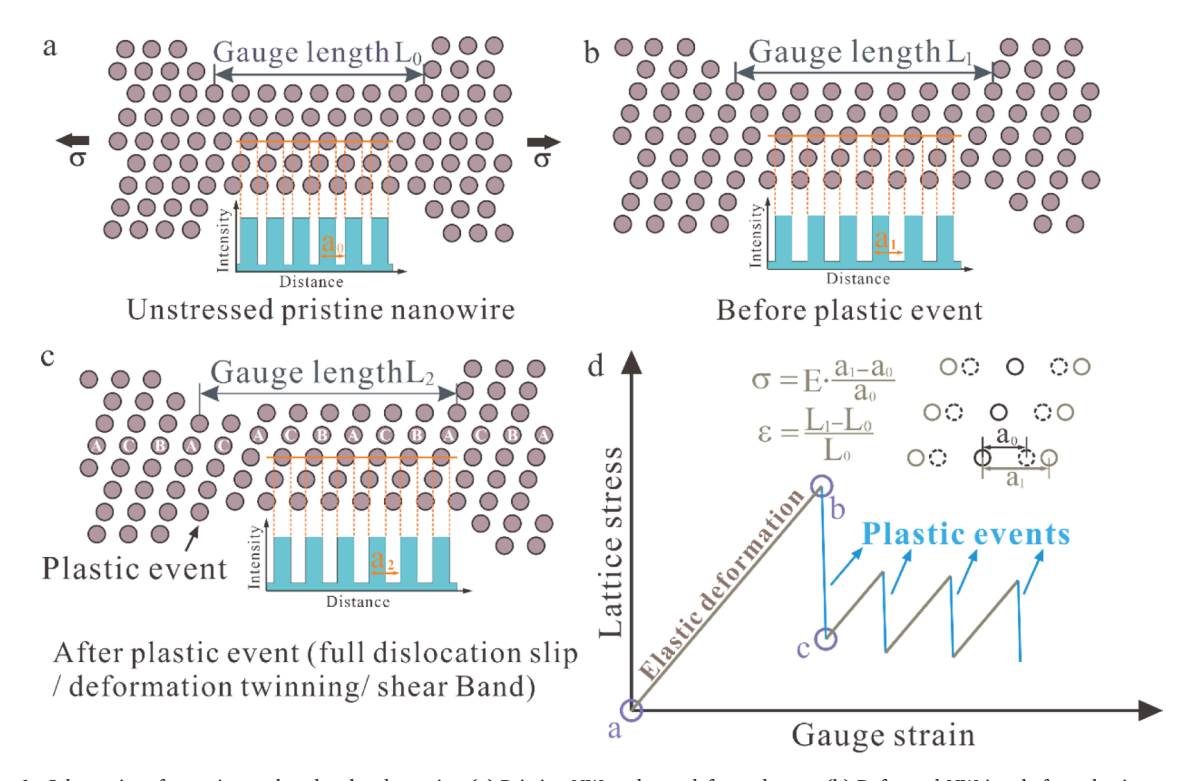


Fig. 1. Schematics of experimental molecular dynamics. (a) Pristine NW under undeformed state. (b) Deformed NW just before plastic event. (c) Deformed NW after an atomic-scale plastic event. (d). Lattice stress versus gauge strain curve; points (a–c) indicate the states of deformation shown in the images of a–c.

2014; Schwaiger and Kraft, 1999; Xu and Zhu, 2012), their mechanical reliability, a precondition for nanoscale devices to function well, has attracted a great deal of scientific and technological interests. The particularly small specimen size and the lack of ultra-low force load cell and reliable clamping method make investigating the mechanical properties of nanoscale crystals difficult (Zheng and Mao, 2021; Zheng et al., 2018; Zheng et al., 2020). Recently, MEMS-based *in situ* experimental mechanics, which is capable of measuring load with nano-Newton resolution and displacement with nanometer resolution (Chen et al., 2015; Ramachandramoorthy et al., 2015a; Zhu, 2017), have been developed to investigate the mechanical properties and deformation behaviors of nanostructured metals under a wide range of strain rates from 10⁻⁵ to 10² s⁻¹ (Chen et al., 2014; Li et al., 2020) and at different experimental temperatures (90–974 K) (Chang and Zhu, 2013; Chen et al., 2014; Kang and Saif, 2011). This experimental method, however, was hard to capture high-quality atomic imaging, failing to obtain the one to one correspondence between atomic-scale deformation processes and stress-strain behaviors in nanoscale metals. In addition, it highly relies on complicated setups making their implementations and operations both challenging and expensive (Lu and Lou, 2011).

Here, we propose an experimental method for nanoscale metals based on *in situ* atomic-scale experimental mechanics with HRTEM, that is called experimental molecular dynamics, which is capable of directly relating individual atomic-scale plastic events to their stress-strain responses in nanoscale metals based on *in situ* atomic-scale observation. In experimental molecular dynamics, the stresses (σ) in crystal lattice, that is yield strength and flow stresses during deformation, can be determined at the atomic scale by comparing the difference in interplanar spacings between the unstressed and deformed states (Fig. 1(a,b)), which can be expressed as (Wang et al., 2015b; Zhong et al., 2017)

$$\sigma = E \cdot \frac{a_1 - a_0}{a_0},\tag{1}$$

where a_0 and a_1 are the interplanar spacings perpendicular to the loading direction in the unstressed and deformed NWs, respectively, which can be determined directly during *in situ* experiments, and *E* is the calculated orientation-dependent Young's modulus of a single crystal (Zhang et al., 2020) (see Supplementary Section 2). Since the contrast of the area inside the atomic column is much larger than that outside atomic column, there exists an intensity profile along the loading direction, as shown in Fig. 1(a–c). Based on the intensity profile of the atomic columns, the interplanar spacing, that is the lattice stress during deformation, can be determined accurately (Fig. 1(a–c)). In addition, the applied loading strain (ε) can be expressed as

$$\varepsilon = \frac{L_1 - L_0}{L_0},\tag{2}$$

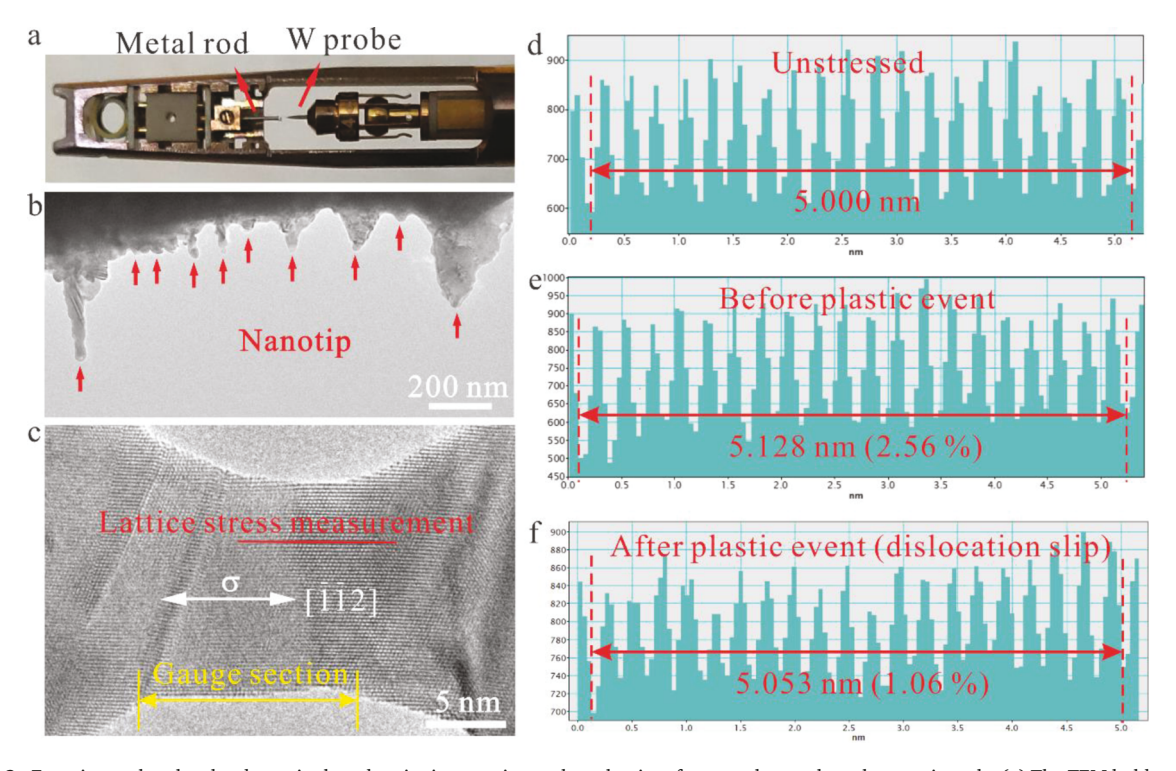


Fig. 2. Experimental molecular dynamics based on *in situ* experimental mechanics of nanoscale metals at the atomic scale. (a) The TEM holder with fractured metallic rods and W probe loaded onto the static side and probe side, respectively. (b) Numerous nanoscale tips after cutting. (c) An example of the fabricated Ag NW. The 20-planes measurement of the lattice spacing along [112] loading is (d) 5.000 nm in pristine Ag NW, (e) 5.128 nm in deformed Ag NW just before the yielding point, and (f) 5.053 nm in deformed Ag NW after plastic event (dislocation slip).

where L_0 and L_1 are the gauge lengths of the unstressed and deformed NWs, respectively, which can be measured directly during *in situ* observation. The gauge section was determined via tracking the shape evolution of the NW (Supplementary Section 1). When the NW firstly experienced an elastic deformation, the lattice stress of the NW increased linearly with the applied strain (from point a to b in Fig. 1(d)). As the lattice stress in the NW increased to the critical stress (point b in Fig. 1(d)), a plastic event, such as full dislocation slip, deformation twinning and shear band, was activated to contribute to plastic strain. Such strain resulted in the partial release of the elastic strain energy accumulated in the crystal lattice and thus a significant stress drop in the applied load (from point b to c in Fig. 1 (d)), due to the displacement-controlled loading scheme (Cao et al., 2008; Kiener and Minor, 2011). Consequently, the lattice stress decreased from $\sigma_1 = E \cdot \frac{a_1 - a_0}{a_0}$ to $\sigma_2 = E \cdot \frac{a_2 - a_0}{a_0}$, and the gauge stain increased to $\varepsilon_2 = \frac{L_2 - L_0}{L_0}$. During further deformation, the plastic flow process of the nanoscale metal was mediated by alternating elastic deformations (stress rises) and individual atomic-scale plastic events (stress drops), as shown in Fig. 1(d). Using the methods mentioned above, one to one correspondence between atomic-scale deformation processes and stress-strain states in nanoscale metals can be obtained during the whole process of deformation. Experimental molecular dynamics is thus expected to be an effective and feasible method to validate stress-based modeling of plastic deformation, and verifies computational mechanics based on MD simulations.

In this work, the in situ tensile tests with HRTEM were performed inside a FEI Tecnai F30 TEM and a FEI Titian 80-300 TEM using a Nanofactory scanning tunneling microscope (STM) holder. Before the in situ tests, the metallic nano-tips were generated at the clean fracture surface of a high-purity (99.999%) bulk metal rod using a wire cutter. Subsequently, the metal rod with nanotips was loaded onto the static side of the TEM holder (Fig. 2(a,b)). The tungsten (W) probe was mounted onto the STM platform, and thus acted as a piezo-controlled STM probe with angstrom precision (Fig. 2(a)). Via controlling the movement of the W probe to contact with the selected nano-tip with viewing directions along low-index zone axes (for example < 110 > for FCC, < 110 > and < 111 > for BCC and < 1120 > for HCP), the nano-tip and the W probe were welded together by applying either an electric pulse or a constant voltage, and then a single-crystalline nanowire (NW) was formed (Cao et al., 2018; Wang et al., 2018c). The applied strain rate during mechanical testing was controlled by the movement speed of the piezo-manipulator of the STM holder. The in situ nanofabrication in this study can generate single-crystalline NW with clean surface and controllable dimension, which is ideal for studying discrete plastic events at atomic scale. The middle segment of the bridge-shaped single crystals had a smaller diameter compared to those at either end, and therefore concentrated all plastic deformation during mechanical testing, serving as the gauge section (Fig. 2(c)). The gauge lengths for the < 001 >-oriented gold (Au), < 112 >-oriented silver (Ag), < 110 >-oriented W, < 1110 >-oriented rhenium (Re) and < 112 >-oriented W single-crystalline NWs adopted in this study (Supplementary Figs. 2-6) were defined based on the selection criterion of gauge section (see Supplementary Section 1). Considering the small diameter variation and the circular cross-sectional shape in the gauge section (Wang et al., 2015b), the thicknesses were approximately uniform across the sample.

To analyze the lattice stress evolution during the deformation process, the lattice spacings were measured in a TEM software of DigitalMicrograph® developed by Gatan Inc. The elastic strain in the crystal lattice can be determined at the atomic scale by comparing the difference in interplanar spacings over 20 atomic planes between the unstressed (Fig. 2(d)) and deformed states (Fig. 2 (e–f)). To minimize measurement errors, repeated 20-planes measurements were conducted at different locations in the gauge section with small diameter variation. Given that the Young's modulus and the applied force were constant in the NW upon mechanical loading, thickness/diameter variation in the gauge section, if any, could cause that lattice strain (stress) change slightly along the loading direction, which is included in the error bars of lattice stress measurement. For instance, the measured (111) interplanar spacing of $[\overline{112}]$ -oriented Ag NW changed continuously from 5.000 nm under unstressed state (Fig. 2(d)) to 5.128 nm before dislocation slip (Fig. 2(e)) and finally to 5.053 nm after dislocation slip (Fig. 2(f)). Consequently, the critical lattice stress for activating a single plastic event (full dislocation slip) was 2.15 GPa, which was calculated by multiplying the lattice strain of 2.56% with the Young's modulus of 84.1 GPa under $[\overline{112}]$ tensile loading (Zhong et al., 2017). After a plastic event, lattice stress decreased significantly from 2.15 to 0.91 GPa (2.56 and 1.08%) under a fixed displacement rate. In addition, the applied strain can be determined via monitoring the change of the gauge length. Consequently, the stress-strain responses, associated with elastic and plastic deformation in nanoscale metals, can be evaluated during the whole process of deformation.

2.2. Molecular dynamics simulations

MD simulations were conducted using the software Large-scale Atomic/Molecular Massively Parallel Simulator (LAMMPS) (Plimpton, 1995). The interatomic interaction of Ag metal was simulated with the embedded atom method (EAM) potentials by Wu and Trinkle (2009). A rectangular Ag NW oriented along $[\overline{11}2]$, [111] and $[1\overline{1}0]$ directions with a gauge length of 9.1 nm was modeled, and the cross-section areas of the gauge section equaled to 4×2 nm². The long axis and loading direction were oriented along $[\overline{11}2]$ direction the same as that in experiments. The strain rate of 10^5 s⁻¹ was studied. The energy of the models was minimized by the conjugate gradient method, and then relaxed for 100 ps under zero pressure using an isothermal–isobaric (NPT) ensemble with a Nose-Hoover thermostat at 300 K. Following relaxation, tensile deformation at the same temperature was carried out by stretching the simulation box along the $[\overline{11}2]$ direction at a constant engineering strain rate in the NVT ensemble. The undeformed atomic volume was used to calculate the axial stress in the NWs. Atomic-level snapshots of NW during deformation were studied by the common neighbor analysis (CNA) using the software OVITO (Stukowski and Albe, 2010).

3. Full dislocation slip-based plastic event

Owing to the pronounced surface effect caused by ultrahigh surface-to-volume ratio of nanoscale metals, the mechanical behaviors of materials at the nanoscale significantly deviate from their bulk counterparts (Li et al., 2018; Li and Ma, 2018). As is well known, dislocation nucleation mechanism, controlling strength, is demonstrated to be size-dependent. In bulk materials, dislocations were usually generated by Frank-Read source (Anderson et al., 2017), grain boundary (GB) (Schiøtz and Jacobsen, 2003; Yamakov et al., 2004), the intersection between twin boundary (TB) and GB (Frøseth et al., 2004; Li et al., 2010b; Lu et al., 2009a; Lu et al., 2009b). In submicro/micro-sized single metallic crystals, plasticity was mediated through the activation of single-arm dislocation source (or truncated Frank-Read source) (Chisholm et al., 2012) (Kiener and Minor, 2011) (Oh et al., 2009). As sample size further decreased to nanoscale, the free surface of nanocrystals, serving as both the source and drain for dislocations, mediated plastic deformation, as frequently reported in MD studies (Li et al., 2018; Weinberger and Cai, 2008; Weinberger et al., 2012; Zhu et al., 2008). Our experimental research on the tensile test of Au NW have proved such conclusion, and the stress-strain responses, related to the individual dislocation activities, were investigated.

Fig. 3 shows the tensile loading of an Au NW loaded along [001] under a strain rate of 10^{-3} s⁻¹ and viewed along [$\overline{1}10$] direction. During mechanical loading, the surface steps, located at the intersection of two sets of $\{111\}$ planes, served as dislocation nucleation sources. At the yielding point, a leading partial nucleated from a favorable surface step, and then propagated through the Au crystal leaving behind a stacking fault (SF), as shown in Fig. 3(a,b). Subsequently, the SF was eliminated by the emission and glide of a trailing partial at the same location, forming a full dislocation (Fig. 3(c)). To further understand the atomistic mechanics of surface dislocation nucleation (SDN), a quantitative lattice strain analysis at the atomic scale was performed on the HRTEM images. Before the nucleation of the leading partial, there existed significant stress concentration in the area close to the surface step, as indicated by the black arrowhead in Fig. 3(d). The favorable stress state enabled the surface step to be a preferable nucleation site. After dislocation nucleation, the localized stress concentration near surface step was reduced, as shown in Fig. 3(e). In addition, the surface areas enclosed by the black boxes in Fig. 3(d,e) were used as lattice strain gauge to investigate the change in lattice strain caused by an individual plastic event at atomic scale. The quantitative strain profile (Fig. 3(f)) also shows that after dislocation nucleation the mean elastic lattice strain decreased from 0.048 to 0.028, reducing the stress concentration near surface step. Given that the Young's modulus of the [001]-oriented Au NW is 42.3 GPa (Zheng et al., 2010), stress in crystal lattice decreased from 2.03 to 1.18 GPa after the dislocation activity.

Our experimental research on the tensile test of Au NW also demonstrated that the plastic flow process of the Au NW was mediated by alternating dislocation starvation and follow-up dislocation nucleation and glide, resulting in cyclic stress rises and drops under the displacement-controlled loading. As shown in Fig. 4(a), the lattice stress increased with the applied loading strain linearly before yielding. As the lattice stress increased to the yielding point of 1.46 GPa (point a in Fig. 4(g)), a full dislocation nucleated from a surface step, glided through the NW and then annihilated at the opposite free surface, causing the surface step to be thickened by one atomic

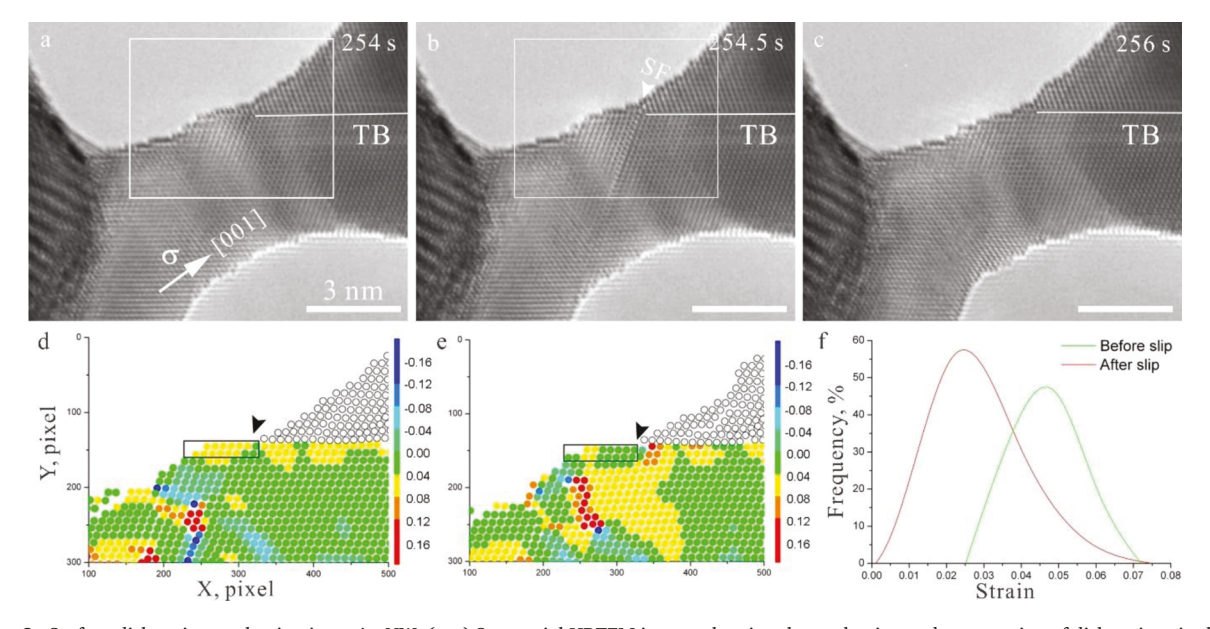


Fig. 3. Surface dislocation nucleation in an Au NW. (a–c) Sequential HRTEM images showing the nucleation and propagation of dislocations in the Au NW under tensile loading along < 001 >-orientation at room temperature under a strain rate of $\sim 10^{-3}$ s⁻¹. Scale bars are 3 nm. (d,e) The strain mapping of the white-boxed area in a and b. The black arrowheads indicate the nucleation site for dislocation. Open circles represent the twinning lamella. (f) A quantitative strain analysis of the lattice strain gauge (black-boxed region in d and e); frequency is the number of atoms with that strain divided by the total number of atoms in the lattice strain gauge. Source: (a–f) reprinted with the permission from Ref. (Zheng et al., 2010). © 2015, Nature Publishing Group.

layer (Fig. 4(a,b)). Furthermore, the plastic event of full dislocation slip in Au NW under displacement-controlled loading resulted in the partial release of the elastic strain energy accumulated in the crystal lattice and thus the significant stress drop in the applied load (from the point a of 1.46 GPa to the point b of 0.90 GPa in Fig. 4(g)). Owing to "dislocation starvation" in the deformed Au NW (Shan et al., 2008), the subsequent plastic flow process was mediated by the follow-up dislocation nucleation and glide (Fig. 4(c,d) and Fig. 4 (e,f)) rather than the motion of pre-existing dislocations. The surface morphology of Au NW during deformation was changed continuously by the dislocation activities. Each full dislocation slip increased the height of surface step by one atomic layer (Figs. 4(d) and 4(f)), and caused a significant stress drop in Au NW at the second (the point c of 1.40 GPa in Fig. 4(g)) and the third (the point e of 1.44 GPa in Fig. 4(g)) yielding point. Such alternating stress rise and drop, caused by elastic deformation and full dislocation slip respectively, is in consistent with previous MD studies in nickel (Ni) NW (Shan et al., 2007), copper (Cu) NW (Rohith et al., 2018) and Au NW (Lu et al., 2011; Rabkin and Srolovitz, 2007).

The plastic strain, induced by an individual full dislocation activity in the [001]-orientated Au NW, was quantitatively calculated as follows to verify the rationality of experimental molecular dynamics. The Burgers vectors of the activated full dislocations with largest Schmid factor on (111) were $\frac{1}{2}[\bar{1}01]a$ or $\frac{1}{2}[0\bar{1}1]a$, where a is the lattice constant (4.08 Å for Au (Ogata et al., 2004)). The slip and annihilation of each full dislocation contributed to an axial elongation of $\frac{1}{2}a$, based on the components of full dislocation Burgers vector along the [001] axial direction. Hence, the theoretical plastic strain, accommodated by each full dislocation activity, was $\frac{1}{2}\frac{a}{L_0}$, where L_0 was the initial gauge length. Under the displacement-controlled loading, such plastic strain contributed to the decrease in the applied load (stress drop) and the increase in gauge strain. The experimentally measured plastic strain, accommodated by an individual plastic event, can be expressed as

$$\varepsilon = \frac{\sigma_1 - \sigma_2}{E} + \frac{L_2 - L_1}{L_0},\tag{3}$$

where σ_1 and σ_2 are the stresses inside the crystal lattice before and after a plastic event, respectively. L_1 and L_2 are the gauge lengths before and after a plastic event. In this work, the initial gauge length for [001]-oriented Au NW is 9.1 nm (Fig. 4(a)). The experimental and theoretical plastic strains, induced by individual full dislocation activities, were sumarized in Table 1. The mean value of absolute errors between the theoretical and experimental strains is 0.13%, verifying that the proposed evaluation method for investigating the stress-strain curves in nanoscale metals in this work is feasible and accurate.

The size-dependent stresses required to activate a partial dislocation (σ_P) and a perfect dislocation (σ_F) are given by (Chen et al., 2003; Hwang et al., 2015)

$$\sigma_{\rm P} = \frac{1}{\rm s} \left(\frac{2\alpha\mu b_{\rm P}}{\rm D} + \frac{\gamma_{\rm SF}}{b_{\rm P}} \right),\tag{4}$$

$$\sigma_{\rm F} = \frac{1}{\rm s} \left(\frac{2\alpha\mu b_{\rm N}}{\rm D} \right),\tag{5}$$

where *D* is the sample size, *s* is the Schmid factor, μ is the shear modulus, γ_{SF} is the stacking fault energy, b_P and b_N are the magnitudes of the Burgers vectors for leading partial and full dislocations, respectively, and α are 0.5 and 1.5 for edge and screw dislocations, respectively. For Au NW, μ is 20.9 GPa Ogata et al., 2004), γ_{SF} is 49 mJ/m² (Li et al., 2011b), b_P and b_N are 1.67 and 2.88 Å (Ogata et al., 2004), respectively. The sample sizes of the Au NWs where the leading partial (Fig. 3(a–c)) and full dislocation activities (Fig. 4(a–f)) happened were 4.10 and 2.91 nm, respectively. The Schmid factors for the leading partial and full dislocation were 0.23 and 0.41, respectively. According to Eqs. (4),((5), the critical stresses for activating a leading partial and a full dislocation were 5.24 and 4.87

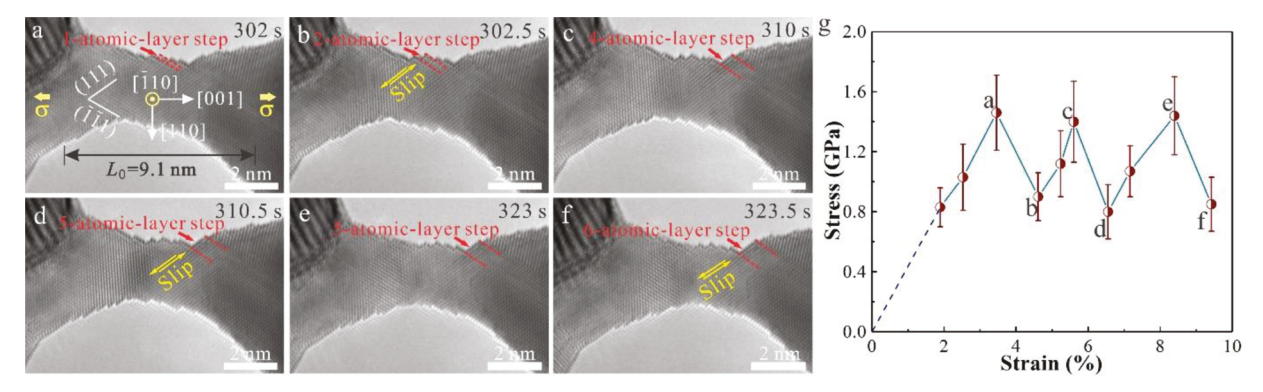


Fig. 4. Full-dislocation-mediated discrete plasticity in an Au NW. (a–f) Sequential HRTEM images showing the plastic deformation process in Au NW, which is controlled by repeated nucleation and propagation of full dislocations. Each full dislocation activity resulted in the surface steps thickened by one atomic layer (b,d,f). (g) Stress-strain curve during tensile loading; points (g–l) indicate the states of deformation shown in the TEM images of a–f. The error bars represent the variations of the measured lattice stresses at different locations of the NW. Source: (a–f) reprinted with the permission from Ref. (Zheng et al., 2010). © 2015, Nature Publishing Group.

Table 1
Experimental and theoretical values of plastic strain caused by individual full dislocation activities in [001]-oriented Au NW.

Sample Stress drop (GPa)	[001]-oriented Au NW Stress drop 1 (1.46–0.90)	Stress drop 2 (1.40-0.80)	Stress drop 3 (1.44–0.85)
Dislocation activity	One Full dislocation	One Full dislocation	One Full dislocation
Experimental strain increment (%)	2.38	2.37	2.39
Theoretical strain increment (%)	2.25	2.25	2.25
Absolute error (%)	0.13	0.12	0.14

GPa, respectively. Considering that the theoretical model neglected some factors contributing to dislocation nucleation (Zhu et al., 2012), the calculated nucleation stresses for the leading and full dislocations were supposed to be larger than those under laboratory conditions. Hence, the calculated result, showing that the nucleation stress for a leading partial is larger than that for a full dislocation, is qualitatively consistent with the stress measured in the experiments (2.03 GPa for the leading partial and 1.46 GPa for the full dislocation). Experimental molecular dynamics for nanoscale metals is an effective method to investigate the individual atomic-scale plastic events and the resultant stress-strain behaviors.

At the final stage of the tensile test, a neck was formed in the central segment of the Au NW, as shown in Fig. 5(a). The measured (001) interplanar spacing of 2.26 Å in the necking region was much larger compared to 2.03 Å outside the necking region. According to Eq. (1), the lattice stress in the necking region was as large as 4.79 GPa, resulting in local stress concentration, which was also demonstrated by the quantitative lattice strain analysis in Fig. 5(c). Such large stress concentration in the necking region contributed to the final fracture of the Au NW, as shown in Fig. 5(b).

4. Deformation twinning-based plastic event

The mechanical properties of polycrystalline metals can be tuned in a wide range via interface engineering (Zhao et al., 2020b; Zheng et al., 2020). Nanotwinned metals usually exhibit excellent mechanical properties with ultrahigh strength and acceptable ductility, compared to their twin-free counterparts (Wang et al., 2015a; Wang et al., 2013b; Zhao et al., 2020a). The twin-thickness-dependent strengthening is associated with the blocking effect of the coherent twin boundaries (CTBs) on full and partial dislocations (Lu et al., 2015; Wang et al., 2015a; Wang et al., 2013b). In addition, the migration of CTB and incoherent twin boundary (ITB) (Kim et al., 2018; Seo et al., 2013; Seo et al., 2011; Wang et al., 2018b), dislocation nucleation from TB (Wang et al., 2017a), TB-assisted dislocation slip (Fu et al., 2018; Wang et al., 2017a), detwinning mechanisms (Cheng et al., 2017; Yin et al., 2020) and TB sliding (Kim et al., 2020; Yue et al., 2017) have been observed to contribute to plasticity in nanoscale metals. Thus far, the twining-related plastic deformation mechanisms have been attracted extensive research interest in the field of material science and engineering. Experimental molecular dynamics opens a window of opportunity for directly characterizing atomic-scale twinning behaviors and the associated stress-strain responses. Deep insights into the atomic-scale mechanisms of deformation twinning are critical for not only fundamental scientific aspect but also advanced materials design.

In FCC NWs, deformation twins initiated and then thickened through layer-by-layer movement of twining partial dislocations emitted from free surface (Li et al., 2011a; Seo et al., 2013; Seo et al., 2011; Zheng et al., 2010). The tensile test of the Ag NW loaded along [$\overline{11}$ 2] under a strain rate of 10^{-3} s $^{-1}$ and viewed along [$\overline{11}$ 0] proved such conclusion. Fig. 6(a,b) shows the elastic deformation process of the Ag NW without any crystal structure change, during which the lattice stress increased with the applied strain linearly, as observed in the tensile test of Au NW. As the lattice stress increased to the yielding point of 3.00 GPa, a leading partial dislocation nucleated at the free surface and then glided though the NW, leaving behind a SF (Fig. 6(c)). Owing to the plastic strain accommodated by the partial dislocation activity, a stress drop could be seen in the stress-strain curve (from the point b of 3.00 GPa to the point c of 2.14 GPa in Fig. 6(g)). As deformation proceeded, a twinning partial dislocation with the same Burgers vector as the first leading

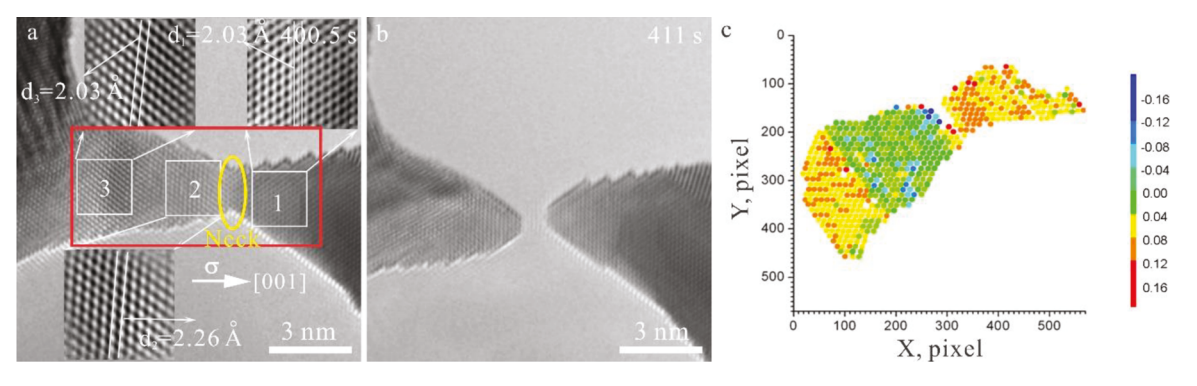


Fig. 5. Neck formation in the tensile test of an Au NW. (a) A neck appeared in the central part of the Au NW. (b) Fracture failure of the Au NW at the final stage of tensile loading. (c) The strain mapping of the red-boxed area in n. Source: (a,b) reprinted with the permission from Ref. (Zheng et al., 2010). © 2015, Nature Publishing Group.

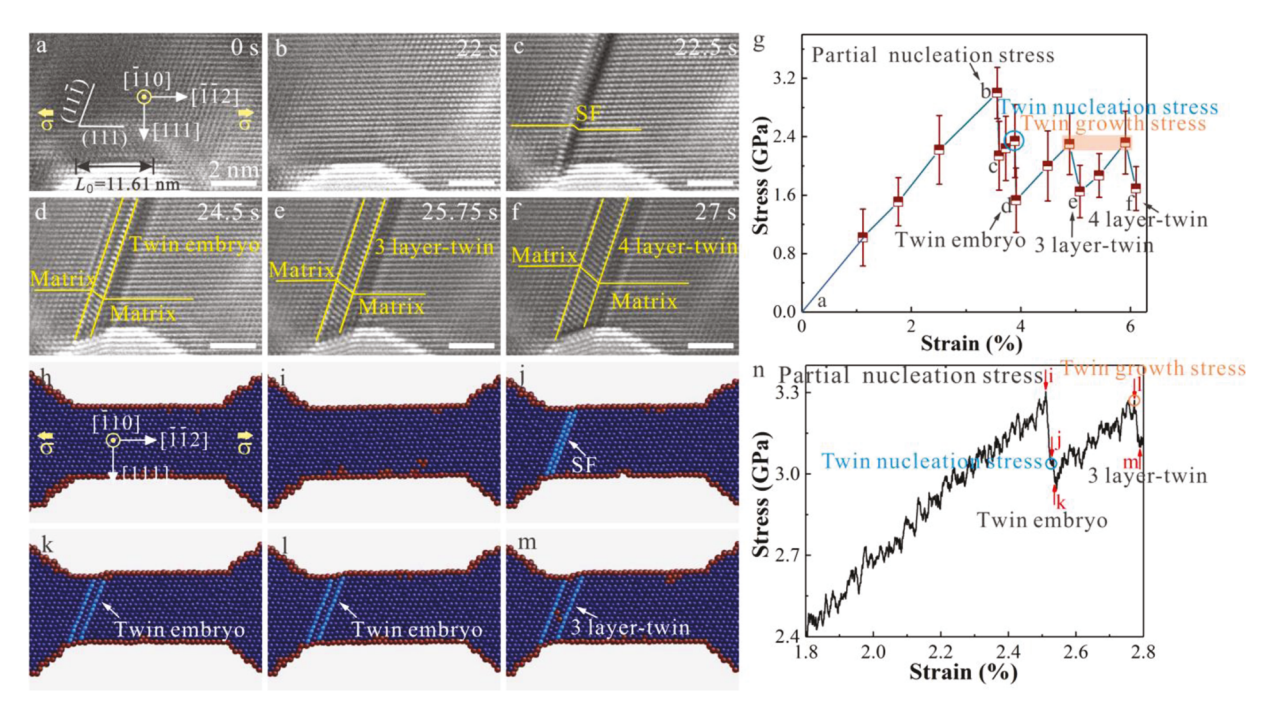


Fig. 6. Deformation-twinning-mediated plasticity in an Ag NW. (a) The pristine Ag NW with a diameter of 15.4 nm as viewed along $[\overline{1}10]$ and loaded along $[\overline{1}\overline{1}2]$ -orientation at room temperature and a strain rate of $\sim 10^{-3}$ s⁻¹. (b) No defect existed in Ag NW before yielding. (c) A leading partial nucleated and propagated through the Ag NW. (d–f) Twin nucleated and expanded in a layer-by-layer method. Scale bars are 2 nm. (g) Stress-strain curve during tensile loading; points (a–f) indicate the states of deformation shown in the TEM images of a–f. The error bars represent the variations of the measured lattice stresses at different locations of the NW. (h) MD simulations of the 4 nm-diameter Ag NW under $[\overline{1}\overline{1}2]$ tension at the temperature of 300 K and a strain rate of 10^5 s⁻¹. (i) elastic deformation in Ag NW before yielding. (j) The nucleation and propagation of a leading partial after yielding. (k–m) Sequential snapshots showing the first and second twinning partial activities in Ag NW. (n) Stress-strain curve during tensile loading; points (i–m) indicate the states of deformation shown in the images of i–m.

partial nucleated and glided adjacent to the first leading partial, resulting in a two-layer SF (Fig. 6(d)), which is called twin embryo (Zhang et al., 2017). During the subsequent loading process, the deformation twin thickened continuously via layer-by-layer movement of twining partials emitted from free surface (Fig. 6(e,f)), as reported by Hwang et al. (2015), Roos et al. (2014), Lee et al. (2014) and Seo et al. (2013, 2011). The critical stresses for activating the first, second and third twinning partial activities were 2.34, 2.30 and 2.32 GPa, respectively. The nucleation and thickening of deformation twin, mediated by twining partials, resulted in discrete stress drops, as observed in the stress-strain curve (Fig. 6(g)).

It should be also noticed that the critical stress for activating a leading partial dislocation activity (3.00 GPa) was larger than those for the twinning partial activities (2.30–2.34 GPa), which can be well-understood in terms of the generalized stacking fault energy (GSFE) (Kibey et al., 2007; Kim et al., 2018; Li et al., 2011b; Van Swygenhoven et al., 2004; Weinberger and Cai, 2012). The critical stress for activating a leading partial activity in a perfect crystal can be expressed as (Weinberger and Cai, 2012)

$$\sigma_{\rm L} = \alpha \gamma_{\rm USF}/({\rm bs}),$$
 (6)

where $\alpha \approx \pi$ is a geometric factor, $\gamma_{\rm USF}$ is the unstable stacking fault (USF) energy, b is the partial Burgers vector and s is the Schmid factor of the leading partial. The critical stress for activating a twinning partial activity adjacent to the first leading partial is given by (Weinberger and Cai, 2012)

$$\sigma_{\rm T} = \alpha (\gamma_{\rm UTF} - \gamma_{\rm ISF})/({\rm bs}), \tag{7}$$

where γ_{UTF} is the unstable twinning fault (UTF) energy and γ_{ISF} is the intrinsic stacking fault (ISF) energy. For Ag, the γ_{USF} , γ_{UTF} and γ_{ISF} is 91 mJ/m², 100 mJ/m² and 16 mJ/m², respectively Jin et al., 2011), the Schmid factor is 0.31, and the Burgers vector for partial is 1.64 Å. According to Eqs. (6),((7), the critical stresses for activating a leading partial and a twinning partial activity are 5.62 and 5.19 GPa, respectively. The critical stress for activating a leading partial is larger than that for a twinning partial, which is qualitatively consistent with our experimental results. The discrepancy that the theoretically calculated stresses are larger than the experimental ones is presumably due to the fact that the GSFE-based model is not rigorously modeled and neglects the well-known size effect in nanostructured metals (Zhu et al., 2012).

The theoretical plastic strains, accommodated by the individual partial dislocation activities, were calculated as follows to further verify the feasibility of experimental molecular dynamics. The activated partial dislocations in the $[\overline{112}]$ -oriented Ag NW were

 $\frac{1}{6}[\overline{2}1\overline{1}]a$ on $(11\overline{1})$ plane or $\frac{1}{6}[\overline{0}2\overline{1}]a$ on $(11\overline{1})$ plane, where a is the lattice constant (4.02 Å for Ag (Ogata et al., 2004)). Based on Burgers vector component along the $[\overline{1}12]$ direction, each partial dislocation activity theoretically contributed to an axial plastic strain of $\frac{\sqrt{6}}{36}\frac{a}{L_0}$, where L_0 was the initial gauge length (11.61 nm for the $[\overline{1}12]$ -oriented Ag NW). According to Eq. (3), the stress-strain behaviors and the change in gauge strain, partial dislocation-induced plastic strains can be experimentally obtained (Table 2). The mean value of the absolute errors between the theoretical and experimental plastic strain are less than 0.18%.

To further understand the twinning behaviors and the resultant stress-strain responses, a 4 nm-diameter Ag NW was strained in tension along $[\overline{11}2]$ direction at room temperature and a strain rate of 10^5 s⁻¹ by MD simulation, as shown in Fig. 6(h-q). The Ag NW initially experienced elastic deformation (Fig. 6(h,i)), and then a SF was induced in the NW via the nucleation and propagation of a leading partial (Fig. 6(j)) after yielding, causing a stress drop from 3.30 to 3.05 GPa. Subsequently, the deformation of the Ag NW was mediated by twinning partials, resulting in the nucleation (Fig. 6(k)) and growth (Fig. 6(m)) of twin. The critical stress for activating a leading partial dislocation activity (3.30 GPa) is larger, compared to the twinning partials (3.05–3.26 GPa), which qualitatively coincided with our experimental results and the theoretical calculations. Furthermore, Fig. 6(n) shows that the first and second twinning partial dislocation activities resulted in the stress drops of 0.10 GPa (from point j to k) and 0.16 GPa (from point l to m), respectively, similar to our experimental observations of dislocation-slip-induced stress drop (Fig. 6(g)).

It has been well documented that full dislocation slip was the dominant deformation mechanism in molybdenum (Mo) (Brinckmann et al., 2008; Huang et al., 2011; Kim et al., 2010; Schneider et al., 2009), W (Kim et al., 2010; Schneider et al., 2009), tantalum (Ta) (Kim et al., 2010; Schneider et al., 2009) and niobium (Nb) (Kim et al., 2010; Schneider et al., 2009) sub-micrometer pillars with BCC structure at room temperature. When the sample size decreased to a few of tens of nanometer, deformation twinning dominated over full dislocation slip to mediate plasticity in BCC NWs (Wang et al., 2015b; Wang et al., 2018c; Wei et al., 2019). In BCC NWs, the progress of twin nucleation and thickening was quite similar to that in an FCC NW. Such phenomenon was observed in the compression test of the W bicrystal NW loaded along $[\bar{1}10]$ under a strain rate of 10^{-3} s $^{-1}$ and viewed along [110] (Fig. 7). The Young's modulus of the W NW with a gauge length of 30.63 nm is 389 GPa (Wang et al., 2015b). The W NW firstly underwent elastic deformation (Fig. 7(a, b)), before the yielding point (point b in Fig. 7(g)). As the lattice stress increased to 19.80 GPa, a twin embryo nucleated from the intersection between the GB and free surface, and then laterally penetrated the whole NW (Fig. 7(c)), resulting in a prestigious stress drop in the applied load (from the point b of 19.80 GPa to the point c of 5.02 GPa in Fig. 7(g)) and the increase in the gauge strain (3.62%). Upon further loading, the twin embryo vertically thickened through the layer-by-layer movement of $1/6[1\overline{1}1]$ twinning partials on a series of adjacent ($\overline{1}12$) planes contributing to plastic strain (Fig. 7(d-f)), and the critical stress for twin growth shows small fluctuations about a constant mean value of 4.75 GPa (from point c to f in Fig. 7(g)). The critical stresses for activating twin nucleation (19.80 GPa) and growth (4.75 GPa) were of the same order of magnitude as the experimental values for twin nucleation (19.2 GPa) and growth (5.0 GPa) in W NW reported by Wang et al. (2015b). It was of additional note that there was a significant difference between twin nucleation and growth stress, which was in accordance with previous MD studies in the tensile loading of BCC NWs (Li et al., 2010a; Sainath et al., 2015; Sainath and Choudhary, 2016; Wang et al., 2011). Different from the W NW, the twin nucleation stress (2.34–3.00 GPa) was at the same level as the twin growth stresses (2.30–2.32 GPa) in Ag NW. The different twinning behaviors in FCC and BCC NWs can be well-understood in terms of GSFE. The energy barrier for emitting the first partial dislocation in W (773 mJ/m²) is much larger compared to Ag (91 mJ/m²) (Li et al., 2010a). Given that the emission of the first partial dislocation was the first step for twin nucleation, W NW required a larger driving force for activating twin nucleation compared to Ag NW. In addition, W NW had a low energy barrier for twin migration (21 mJ/m²) compared to twin nucleation (Li et al., 2010a), causing that the critical stresses for activating twin growth were rather low compared to the twin nucleation stress. In contrast to W NW, the energy barrier for twin growth in Ag NW was close to that for twin nucleation. Thus, the critical stresses for twin nucleation and growth in Ag NW were nearly at the same level.

Different from the classical twinning routes in NWs with cubic structure, deformation twinning in Re was mediated by prismatic (P)-to-basal (B) transformation, as shown in Fig. 8. A $\{10\overline{1}2\}$ twin embryo nucleated from the GB of Re bi-crystal loaded along $[\overline{1}100]$ under a strain rate of $\sim 10^{-3}$ s $^{-1}$ and viewed along $[11\overline{2}0]$ (Fig. 8(a,c)). The Young's modulus of the Re NW with a gauge length of 10.33 nm is 474 GPa (Tromans, 2011). Owing to the incipient plastic strain accommodated by twin nucleation, a significant stress drop could be seen in the stress-strain curve (from the point b of 6.53 GPa to the point c of 3.64 GPa in Fig. 8(g)). Subsequently, the twin embryo grew by the formation and lateral expansion of new basal layers on the twin/matrix interface (Fig. 8(d,e)), as reported by Liu et al. (2014) in submicron-sized single-crystal magnesium (Mg) pillar. As the newly formed twin penetrated through the direction of sample thickness, the atomic-resolution image of the twin embryo was captured without any Moiré fringes, as shown in Fig. 8(f). The laterally expanding layers were indeed basal planes, demonstrating the twinning process in Re NW was mediated by the disconnections on the B|P interfaces instead of twinning dislocations (He et al., 2020). Besides, the step height of most of these disconnections was two

Table 2Experimental and theoretical values of plastic strain caused by deformation twinning in [112]-oriented Ag NW.

Sample	$[\overline{11}2]$ -oriented Ag NW			
Stress drop (GPa)	Stress drop 1 (3.00-2.14)	Stress drop 2 (2.34-1.53)	Stress drop 3 (2.30-1.65)	Stress drop 4 (2.32–1.69)
Dislocation activity	One leading partial	First twinning partial	Second twinning partial	Third twinning partial
Experimental strain increment (%)	0.98	0.97	0.96	0.94
Theoretical strain increment (%)	0.80	0.80	0.80	0.80
Absolute error (%)	0.18	0.17	0.16	0.14

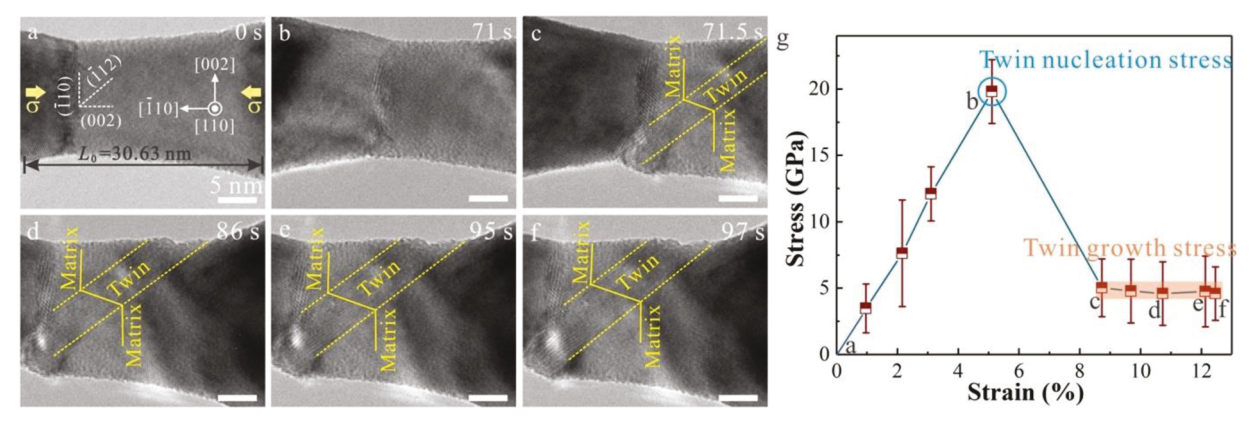


Fig. 7. Compression deformation-induced deformation twinning in a W NW. (a) The pristine W bicrystal nanowire with a diameter of 14.7 nm as viewed along [110] under a strain rate of $\sim 10^{-3}$ s $^{-1}$ and loaded along [$\overline{1}10$]. (b) W NW before yielding. (c–f) Under compression, the deformation twin nucleated and expanded in a layer-by-layer method. Scale bars are 5 nm. (g) Stress-strain curve during compression; points (a–f) indicate the states of deformation shown in the TEM images of a–f. The error bars represent the variations of the measured lattice stresses at different locations of the NW. Source: (a–f) reprinted with the permission from Ref. (Wang et al., 2015b). © 2015, Nature Publishing Group.

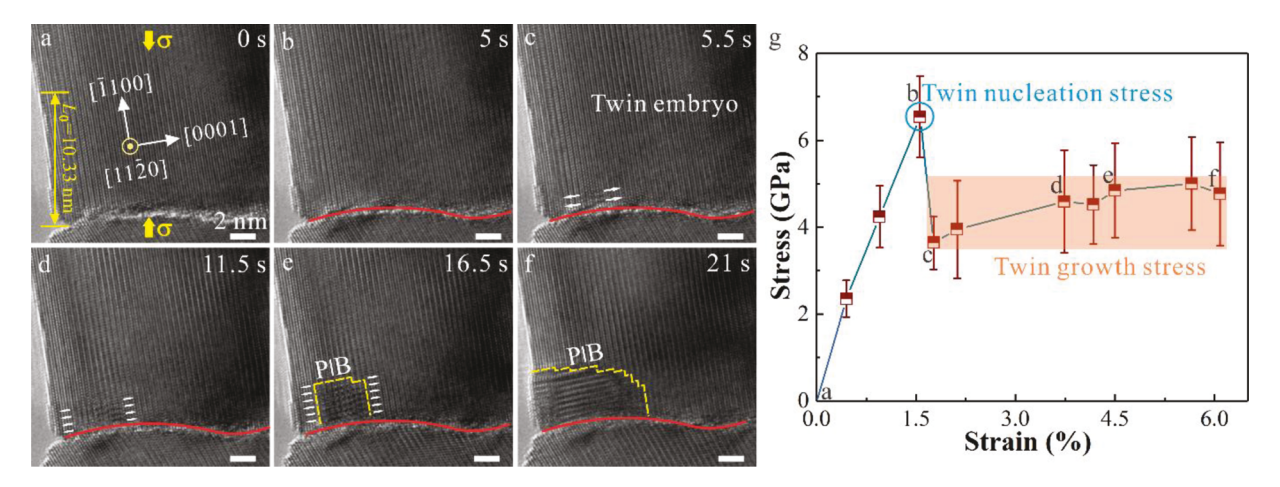


Fig. 8. Prismatic-to-basal transformation-induced deformation twinning in a Re NW. (a) The pristine Re NW loaded along [$\overline{1}110$] under a strain rate of $\sim 10^{-3}$ s $^{-1}$ and viewed along [$11\overline{2}0$]. Red line indicates the GB. (b) Re NW before yielding. (c-f) Sequential HRTEM images showing twin nucleation and expansion in Re NW. Arrows indicate the expansion of basal layers. Yellow lines indicate the B|P interfaces between the twin and matrix. All scale bars are 2 nm. (g) Stress-strain curve during compressive loading; points (a-f) indicate the states of deformation shown in the TEM images of a-f. The error bars represent the variations of the measured lattice stresses at different locations of the NW. Source: (a-f) reprinted with the permission from Ref. (He et al., 2020). © 2020, Nature Publishing Group.

atomic layers. During the process of twin growth, the critical stresses for activating twin expansion increased slowly with applied strain (from the point d of 4.59 GPa to the point f of 4.77 GPa in Fig. 8(g)), which were lower than the twin nucleation stress.

5. Shear band-based plastic event

BCC nanostructured metals with high strength and excellent high temperature performance hold promising potential for applications in small-sized devices under extreme loading conditions (Wang et al., 2018a; Wang et al., 2020a). Compared to nanoscale FCC metals, the atomic-scale deformation process in nanosized BCC metals remains poorly understood, especially at the atomic scale, owing to the lack of effective experimental methods in fabricating and testing the nanoscale BCC metals (Zheng and Mao, 2021). Enabled by the recent advance in TEM-based *in situ* nanomechanical testing, atomic-scale deformation mechanisms, including surface dislocation nucleation, dislocation slip and deformation twinning, have been revealed in W and Nb NWs (Wang et al., 2018a; Wang et al., 2015b; Wang et al., 2020a; Wang et al., 2018c; Wang et al., 2020b; Wei et al., 2019). Moreover, sequential BCC-FCC-BCC phase transformation coupled with shear deformation has been uncovered in the Nb NWs under tensile loading (Wang et al., 2018c) and in the region ahead of a crack tip in Mo thin film (Wang et al., 2014). To date, the one to one correspondence between atomic-scale deformation processes and stress-strain behaviors in nanoscale BCC metals, however, remained largely unexplored.

Our research presents the atomic-scale dynamic processes of dislocation- and shear band- mediated plasticity and the resultant mechanical response in the compression test of the W bicrystal NW loaded along [112] under a strain rate of $\sim 10^{-3}$ s $^{-1}$ and viewed along [111]. The Young's modulus of [112]-oriented W NW is 389 GPa (Wang et al., 2015b), Before compression test, the initial gauge length of the W NW was 28.76 nm, and the pristine W NW was defect free (Fig. 9(a)). During the compression test, the applied loading caused the elastic strain accumulation in the NW, finally resulting in the yielding of the NW via dislocation nucleation from free surface (Fig. 9(b)). Owing to the dislocation activities during yielding, a significant stress drop was observed in the stress-strain curve (from the yielding point of 16.29 GPa to the point b of 14.90 GPa in Fig. 9(g)), which was qualitatively consistent with full-dislocation-slip-induced stress drop reported in the previous MD study of the tensile loading of Mo NW (Wang et al., 2011). During further compressive loading, dislocations continuously nucleated from multiple surface sites (Fig. 9(c)). Most of the newly nucleated dislocations were observed to be dislocation dipoles, which should be half dislocation loops on (101) planes. Due to the large amounts of dislocation nucleation and the low mobility of dislocations in metals with BCC structure (Gumbsch et al., 1998), dislocation density in the W NW increased with the applied strain significantly (Fig. 9(b,c)). Accompanied with the occurrence of significant dislocation slips in the W NW, the stress decreased with applied strain (from the point b of 14.90 GPa to the point c of 12.83 GPa in Fig. 9(g)). Plenty of dislocation activities finally resulted in the sudden nucleation of a shear band at high deformation strain (Fig. 9(d)), causing obvious strain softening (from the shear band nucleation stress of 13.73 GPa to the point d of 3.87 GPa in Fig. 9(g)) and the increase in the gauge strain (4.58%). The shear-band-induced strain softening observed here was similar to the deformation bands accompanied by significant stress drops previously reported in the compression of BCC nanopillars (Huang et al., 2011; Kim et al., 2010). After nucleation, the shear band discretely thickened via dislocation activities on (101) slip planes near the shear band interface unlike the layer-by-layer twinning route frequently observed in FCC and BCC metals (Fig. 9(e,f)), which contributed to large plastic stain to accommodate compression deformation. During the process of shear band thickening, the stress fluctuated with further increase of the strain, and the critical stresses for shear band thickening (from the point e of 5.97 GPa to the point f of 4.37 GPa in Fig. 9(g)) were much smaller than that for shear band nucleation (13.73 GPa). Such difference may be attributed to the high stress concentration in a deformation affected zone adjacent to the shear band interface, which was resulted from the non-symmetric geometry of the sample with shear band (Wang et al., 2018a). The stress concentration facilitated the nucleation and propagation of dislocations in the shear region at low stress level.

As discussed in the above sections, full dislocation slip and deformation twinning were the activated deformation modes in W NW under < 112 > and < 110 > loading, respectively. The analysis of the resolved shear stresses on deformation twinning (< 111 >{112}) and dislocation slip systems (< 111 >{110}), that is Schmid law, plays a critical role in determining the dominant deformation mechanism (Wang et al., 2015b; Wei et al., 2019). Under < 110 > loading, the largest Schmid factors on deformation twinning systems were 0.47, larger than those of 0.41 on dislocation slip systems, causing that deformation twinning was favored in W NW. By contrast, the Schmid factors of deformation twinning (0.39) were smaller than those of dislocation slip (0.41) under < 112 > loading, causing that the resolved shear stresses for dislocation slip were larger compared to deformation twinning. Besides, the difficulty of the lateral expansion of the twin embryo probably also caused that dislocation slip were favored in the W NW under < 112 > loading (Wang et al., 2015b).

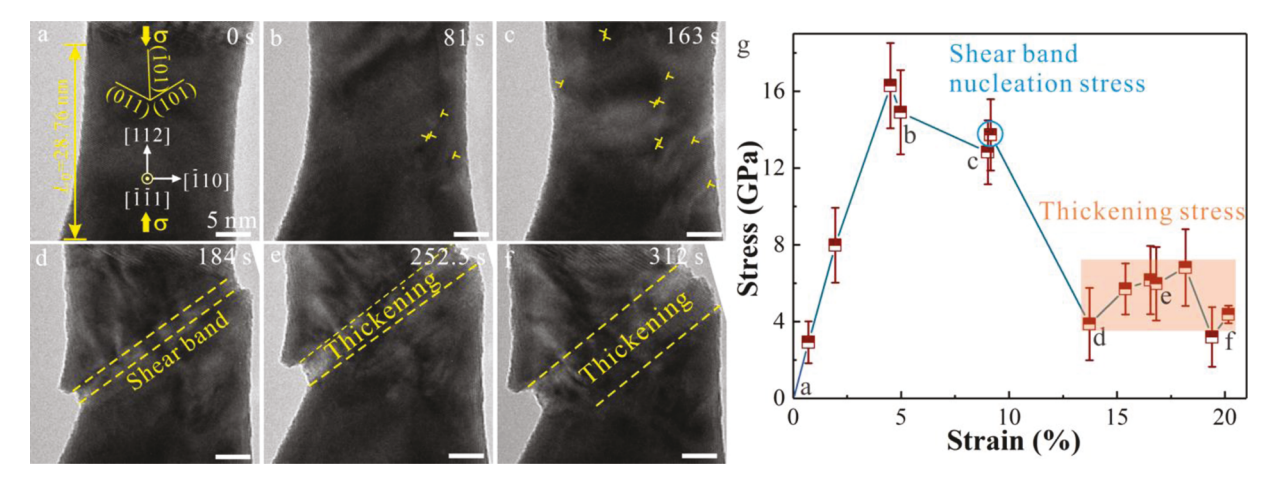


Fig. 9. Dislocation- and shear band-mediated plasticity during the compression of a W NW. (a) Pristine W NW with a diameter of 21 nm as viewed along [$\overline{11}1$] and loaded along [112]-orientation at room temperature and a strain rate of $\sim 10^{-3} \text{ s}^{-1}$. (b,c) A series of TEM images showing the nucleation and propagation of dislocations in the W NW after yielding. (d–f) Sequential TEM images showing the nucleation and expansion of shear band in the deformed W NW. All scale bars are 5 nm. (g) Stress-strain curve during compression corresponding to the sequence in (a)–(f). The error bars represent the variations of the measured lattice stresses at different locations of the NW. Source: (a–f) reprinted with the permission from Ref. (Wang et al., 2015b). © 2015, Nature Publishing Group.

6. Summary and outlook

The rapid development of small-sized electronic devices has brought the mechanical reliability of nanoscale metals to the fore. Experimental molecular dynamics with *in situ* mechanics approach provides a unique opportunity for gaining deep insights into the individual atomic-scale plastic events and the consequent stress-strain behaviors via directly analyzing the change of lattice spacing and gauge length during mechanical loading. We have discussed three plastic events, including full dislocation slip, deformation twinning and shear band, and characterized the resultant stress-strain responses in nanoscale crystals with different crystal structures. The stress drops and strain bursts, characteristics of individual plastic events, are investigated, and the critical stresses for activating the nucleation and growth of atomic-scale defects are obtained. Theoretical analysis on our experimental results, and the comparison between the experimental and computational results reported in the previous studies demonstrate that the approach of experimental molecular dynamics proposed in this work is feasible and effective. The main findings mentioned in above sections are summarized as follows:

- (1) Surface step with localized stress concentration acted as a dislocation nucleation site mediating plastic deformation in an Au NW. Plastic flow was mediated by alternating dislocation starvation and follow-up dislocation nucleation and glide, resulting in cyclic stress rises and drops under the displacement-controlled loading. There existed localized stress concentration in the necking region, causing the final fracture failure the Au NW.
- (2) In Ag and W NWs, deformation twin nucleated and then grew through layer-by-layer movement of partial dislocations emitted from free surface. Compared to a twinning partial, the nucleation stress for a leading partial was larger in Ag NWs. In W NWs, twin nucleation stress was much larger than twin growth stress. The stress-strain behaviors, associated with atomic-scale twinning processes, can be well-understood in terms of the GSFE in metals with cubic structure. In contrast, {1012} twin in Re NW was mediated by P→B transformation instead of twinning dislocations. In Re NW, twin growth stress, lower than twin nucleation stress, increased with the applied strain slightly.
- (3) In the compression test of the W NW, plenty of dislocation activities induced the nucleation of a shear band, resulting in obvious strain softening. Shear band nucleation stress was much larger than shear band growth stresses, which may be attributed to the high stress concentration near the shear band interface caused by the non-symmetric geometry of the sample with shear band.

To date, much scientific and practical interest is currently focused on the mechanical properties and atomic-scale deformation mechanisms in several kinds of nanoscale materials under laboratory conditions, which is a small fraction of what actually happened in practical applications. Deep insights into the atomic-scale plastic events in nanoscale metals and the consequent stress-strain responses under different experimental conditions are critical for not only basic science but also realizing the potential applications of nanoscale metals in the next generation nanodevices. Thus, some interests for future research are enumerated as follows.

- (1) The effects of chemical gas on the mechanical properties of nanoscale metals remain largely unexplored, since the *in situ* TEM nanomechanical tests were usually conducted in vacuum chambers (Sen et al., 2014; Shin et al., 2019). Thus far, the adaptation of *in situ* mechanical testing to gas environmental TEM remains a significant challenge. Very recently, Yin et al. (2019a) performed MEMS-based *in situ* TEM tensile testing of penta-twined Ag NW with hydrogen charging, and they revealed a transition in failure mechanism from distributed plasticity to localized necking in penta-twinned Ag NWs due to the presence of hydrogen around the surface nucleation sites. A thorough understanding of the individual atomistic plastic events and the resultant mechanical responses in nanoscale metals under different chemical atmospheres is of paramount importance for predicting the mechanical reliability of nanostructured metals in a practical application.
- (2) Interface in nanostructured metals plays an important role in mediating deformation. In nanoscale metals with substantial surface area to volume ratio, surface energy, correlated with the aspect ratio, affected the deformation mechanism in operation (Cheng et al., 2017; Filleter et al., 2012; Qin et al., 2015; Ramachandramoorthy et al., 2015b). In metallic multilayered composites, with the layer thickness decreased from sub-microns to few nanometers, the operative mechanism changed from a dislocation pile-up-based Hall–Petch model to confined layer slip of single dislocations and finally to an interface cutting mechanism (Li and Zhang, 2010; Li et al., 2007; Misra et al., 2005; Yan et al., 2013). In nanocrystalline metals, mechanically driven GB migration plays a significant role in deformation processes, including grain growth, recrystallization, phase transformation (Cahn et al., 2006; Luo et al., 2017; Renk et al., 2014; Wang et al., 2017b; Zheng et al., 2020), strongly influencing the mechanical properties of nanostructured metals. To date, atomic-scale deformation mechanisms of interface-mediated plasticity are still in their relatively infancy, because of the complex interface structure (Caillard et al., 2009). Advanced Four-dimensional scanning transmission electron microscopy (4D-STEM) may reveal new atomic-scale mechanisms of interface-mediated plasticity, leading to the solutions of many longstanding puzzles.
- (3) Alloy materials, such as transformation-induced plasticity (TRIP) steels, twinning-induced plasticity (TWIP) steels and highentropy alloys (HEAs) have been designed to achieve a good combination of ultrahigh strength and substantial uniform ductility, which have received much recent attention (Naeem et al., 2020; Zhang et al., 2015; Zhang et al., 2017). Alloying atoms are demonstrated to tune the mechanical properties of alloys via changing their microstructural features. For instance, atomic-scale lattice distortion, caused by the variation in atomic size and electronic structure in a HEA with pronounced compositional inhomogeneity, influences the dislocation behaviors and thus the mechanical properties (Ding et al., 2019; Ma, 2020; Naeem et al., 2020; Wang et al., 2017c). The newly developed energy-dispersive X-ray spectroscopy (EDS) is capable to

- investigate the atomic-scale element distributions in alloys (Ding et al., 2019; Du et al., 2020). *In situ* straining test with advanced EDS should be a promising way to gain atomic-scale insights into the influence of alloying atoms on the deformation mechanisms and mechanical properties, providing new clues for rationally designing high-performance alloys via varying alloy composition.
- (4) Until now, numerous theoretical and experimental investigations have been conducted to study the mechanical properties and atomic-scale deformation behaviors in nanoscale metals under uniaxial loading at room temperature (Wang et al., 2013c; Weinberger and Cai, 2012; Zheng and Mao, 2021; Zhu and Li, 2010). As is well known, the mechanical properties and deformation behaviors of nanoscale metals are size-, strain-rate- and temperature-dependent (Chen et al., 2015; Guo et al., 2015; Sun et al., 2014b; Zhang et al., 2021). The experimental laboratory results are thus difficult to be applied to the nanostructured metals serving under extreme conditions, such as high strain rate, elevated temperature and complex loading. Recently, advanced *in situ* TEM mechanical testing have been developed, which can investigate the NWs under high strain rate at elevated temperature (Chang and Zhu, 2013; Chen et al., 2014; Kang and Saif, 2011; Li et al., 2020). For instance, Cheng et al. (Cheng et al., 2019; Cheng and Zhu, 2020) reported that the crystalline Silicon (Si) NWs under tension are brittle at room temperature but exhibit ductile behavior at high temperatures. Deep insights into atomic-scale plastic events and the resulting stress-strain responses under different experimental conditions could inspire new means to design mechanically stable nanostructured metals to guarantee the reliability of small-scale devices in practical applications.

Declaration of Competing Interest

The authors declare no competing financial interest.

Author contributions

S.Z. conducted the *in situ* TEM experiments and performed the experimental data analysis. S.S. and S.O. carried out the computer simulations. S.Z. and S.X.M. prepared the paper with the contribution of all authors.

Acknowledgments

The authors thank He Zheng and Kui Du for the quantitative lattice strain analysis in the Au NW. S.X.M. acknowledges support from the NSF 1760916 through University of Pittsburgh.

Supplementary materials

Supplementary material associated with this article can be found, in the online version, at doi:10.1016/j.jmps.2021.104687.

Reference

Anderson, P.M., Hirth, J.P., Lothe, J., 2017. Theory of Dislocations. Cambridge University Press, New York, USA. Third ed.

Brinckmann, S., Kim, J.-Y., Greer, J.R., 2008. Fundamental differences in mechanical behavior between two types of crystals at the nanoscale. Phys. Rev. Lett. 100, 155502.

Cahn, J.W., Mishin, Y., Suzuki, A., 2006. Coupling grain boundary motion to shear deformation. Acta Mater. 54, 4953-4975.

Caillard, D., Mompiou, F., Legros, M., 2009. Grain-boundary shear-migration coupling. II. geometrical model for general boundaries. Acta Mater. 57, 2390-2402.

Cao, A., Wei, Y., Mao, S.X., 2008. Alternating starvation of dislocations during plastic yielding in metallic nanowires. Scr. Mater. 59, 219-222.

Cao, G., Wang, J., Du, K., Wang, X., Li, J., Zhang, Z., Mao, S.X., 2018. Superplasticity in gold nanowires through the operation of multiple slip systems. Adv. Funct. Mater. 28, 1805258.

Chang, T.-H., Zhu, Y., 2013. A microelectromechanical system for thermomechanical testing of nanostructures. Appl. Phys. Lett. 103, 263114.

Chen, L.Y., He, M.R., Shin, J., Richter, G., Gianola, D.S., 2015. Measuring surface dislocation nucleation in defect-scarce nanostructures. Nat. Mater. 14, 707–713. Chen, L.Y., Terrab, S., Murphy, K.F., Sullivan, J.P., Cheng, X., Gianola, D.S., 2014. Temperature controlled tensile testing of individual nanowires. Rev. Sci. Instrum. 85, 013901.

Chen, M., Ma, E., Hemker, K.J., Sheng, H., Wang, Y., Cheng, X., 2003. Deformation twinning in nanocrystalline aluminum. Science 300, 1275–1277.

Cheng, G., Yin, S., Chang, T.-H., Richter, G., Gao, H., Zhu, Y., 2017. Anomalous tensile detwinning in twinned nanowires. Phys. Rev. Lett. 119, 256101.

Cheng, G., Zhang, Y., Chang, T.-H., Liu, Q., Chen, L., Lu, W.D., Zhu, T., Zhu, Y., 2019. In situ nano-thermomechanical experiment reveals brittle to ductile transition in silicon nanowires. Nano Lett. 19, 5327–5334.

Cheng, G., Zhu, Y., 2020. *In situ* nano-thermo-mechanical experiment reveals brittle to ductile transition in si nanowires. Microsc. Microscal. 26, 3192–3194. Chisholm, C., Bei, H., Lowry, M., Oh, J., Asif, S.S., Warren, O., Shan, Z., George, E.P., Minor, A.M., 2012. Dislocation starvation and exhaustion hardening in Mo alloy nanofibers. Acta Mater. 60, 2258–2264.

Cui, Z., Han, Y., Huang, Q., Dong, J., Zhu, Y., 2018. Electrohydrodynamic printing of silver nanowires for flexible and stretchable electronics. Nanoscale 10, 6806–6811.

Deng, C., Sansoz, F., 2009. Fundamental differences in the plasticity of periodically twinned nanowires in Au, Ag, Al, Cu, Pb and Ni. Acta Mater. 57, 6090–6101. Ding, Q., Zhang, Y., Chen, X., Fu, X., Chen, D., Chen, S., Gu, L., Wei, F., Bei, H., Gao, Y., 2019. Tuning element distribution, structure and properties by composition in high-entropy alloys. Nature 574, 223–227.

Du, X., Li, W., Chang, H., Yang, T., Duan, G., Wu, B., Huang, J., Chen, F., Liu, C., Chuang, W., 2020. Dual heterogeneous structures lead to ultrahigh strength and uniform ductility in a Co-Cr-Ni medium-entropy alloy. Nat. Commun. 11, 1–7.

Fan, Y., Osetsky, Y.N., Yip, S., Yildiz, B., 2012. Onset mechanism of strain-rate-induced flow stress upturn. Phys. Rev. Lett. 109, 135503.

- Filleter, T., Ryu, S., Kang, K., Yin, J., Bernal, R.A., Sohn, K., Li, S., Huang, J., Cai, W., Espinosa, H.D., 2012. Nucleation-controlled distributed plasticity in pentatwinned silver nanowires. Small 8, 2986–2993.
- Frøseth, A., Derlet, P., Van Swygenhoven, H., 2004. Dislocations emitted from nanocrystalline grain boundaries: nucleation and splitting distance. Acta Mater. 52, 5863–5870
- Fu, X., Wu, X., Yu, Q., 2018. Dislocation plasticity reigns in a traditional twinning-induced plasticity steel by *in situ* observation. Mater. Today Nano 3, 48–53. Gumbsch, P., Riedle, J., Hartmaier, A., Fischmeister, H.F., 1998. Controlling factors for the brittle-to-ductile transition in tungsten single crystals. Science 282, 1293–1295.
- Guo, W., Wang, Z., Li, J., 2015. Diffusive versus displacive contact plasticity of nanoscale asperities: temperature-and velocity-dependent strongest size. Nano Lett. 15, 6582–6585.
- He, Y., Li, B., Wang, C., Mao, S.X., 2020. Direct observation of dual-step twinning nucleation in hexagonal close-packed crystals. Nat. Commun. 11, 1-8.
- Huang, L., Li, Q.-J., Shan, Z.-W., Li, J., Sun, J., Ma, E., 2011. A new regime for mechanical annealing and strong sample-size strengthening in body centred cubic molybdenum. Nat. Commun. 2, 547.
- Hwang, B., Kang, M., Lee, S., Weinberger, C.R., Loya, P., Lou, J., Oh, S.H., Kim, B., Han, S.M., 2015. Effect of surface energy on size-dependent deformation twinning of defect-free Au nanowires. Nanoscale 7, 15657–15664.
- Jin, Z., Dunham, S., Gleiter, H., Hahn, H., Gumbsch, P., 2011. A universal scaling of planar fault energy barriers in face-centered cubic metals. Scr. Mater. 64, 605–608.
- Kang, W., Saif, M.T.A., 2011. A novel SiC MEMS apparatus for *in situ* uniaxial testing of micro/nanomaterials at high temperature. J. Micromech. Microeng. 21, 105017.
- Kibey, S., Liu, J., Johnson, D., Sehitoglu, H., 2007. Predicting twinning stress in fcc metals: linking twin-energy pathways to twin nucleation. Acta Mater. 55, 6843–6851.
- Kiener, D., Minor, A., 2011. Source truncation and exhaustion: insights from quantitative in situ TEM tensile testing. Nano Lett. 11, 3816-3820.
- Kim, J.Y., Jong, D.C., Greer, J.R., 2010. Tensile and compressive behavior of tungsten, molybdenum, tantalum and niobium at the nanoscale. Acta Mater. 58, 2355–2363.
- Kim, S.-H., Kim, H.-K., Seo, J.-H., Whang, D.-M., Ahn, J.-P., Lee, J.-C., 2018. Deformation twinning of ultrahigh strength aluminum nanowire. Acta Mater. 160, 14–21. Kim, S.-H., Park, J.-H., Kim, H.-K., Ahn, J.-P., Whang, D.-M., Lee, J.-C., 2020. Twin boundary sliding in single crystalline Cu and Al nanowires. Acta Mater. 196, 60, 72
- Lee, S., Im, J., Yoo, Y., Bitzek, E., Kiener, D., Richter, G., Kim, B., Oh, S.H., 2014. Reversible cyclic deformation mechanism of gold nanowires by twinning–detwinning transition evidenced from *in situ* TEM. Nat. Commun. 5, 3033.
- Li, B., Li, B., Wang, Y., Sui, M., Ma, E., 2011a. Twinning mechanism via synchronized activation of partial dislocations in face-centered-cubic materials. Scr. Mater. 64, 852–855
- Li, B.Q., Sui, M.L., Mao, S.X., 2011b. Twinnability predication for fcc metals. J. Mater. Sci. Technol. 27, 97-100.
- Li, C., Zhang, D., Cheng, G., Zhu, Y., 2020. Microelectromechanical systems for nanomechanical testing: electrostatic actuation and capacitive sensing for high-strain-rate testing. Exp. Mech. 60, 329–343.
- Li, Q., Xu, B., Hara, S., Li, J., Ma, E., 2018. Sample-size-dependent surface dislocation nucleation in nanoscale crystals. Acta Mater. 145, 19-29.
- Li, Q.J., Ma, E., 2018. When 'smaller is stronger' no longer holds. Mater. Res. Lett. 6, 283-292.
- Li, S.Z., Ding, X.D., Deng, J.K., Lookman, T., Li, J., Ren, X.B., Sun, J., Saxena, A., 2010a. Superelasticity in bcc nanowires by a reversible twinning mechanism. Phys. Rev. B 82, 205435.
- Li, X., Wei, Y., Lu, L., Lu, K., Gao, H., 2010b. Dislocation nucleation governed softening and maximum strength in nano-twinned metals. Nature 464, 877.
- Li, Y.P., Zhang, G.P., 2010. On plasticity and fracture of nano structured Cu/X (X = Au, Cr) multilayers: the effects of length scale and interface/boundary. Acta Mater. 58, 3877–3887.
- Li, Y.P., Zhang, G.P., Wang, W., Tan, J., Zhu, S.J., 2007. On interface strengthening ability in metallic multilayers. Scr. Mater. 57, 117–120.
- Liang, J., Li, L., Tong, K., Ren, Z., Hu, W., Niu, X., Chen, Y., Pei, Q., 2014. Silver nanowire percolation network soldered with graphene oxide at room temperature and its application for fully stretchable polymer light-emitting diodes. ACS Nano 8, 1590–1600.
- Liu, B.-Y., Wang, J., Li, B., Lu, L., Zhang, X.-Y., Shan, Z.-W., Li, J., Jia, C.-L., Sun, J., Ma, E., 2014. Twinning-like lattice reorientation without a crystallographic twinning plane. Nat. Commun. 5, 1–6.
- Lu, L., Chen, X., Huang, X., Lu, K., 2009a. Revealing the maximum strength in nanotwinned copper. Science 323, 607–610.
- Lu, L., Dao, M., Zhu, T., Li, J., 2009b. Size dependence of rate-controlling deformation mechanisms in nanotwinned copper. Scr. Mater. 60, 1062-1066.
- Lu, N., Du, K., Lu, L., Ye, H., 2015. Transition of dislocation nucleation induced by local stress concentration in nanotwinned copper. Nat. Commun. 6, 7648.
- Lu, Y., Lou, J., 2011. Quantitative in-situ nanomechanical characterization of metallic nanowires. JOM 63, 35.
- Lu, Y., Song, J., Huang, J.Y., Lou, J., 2011. Surface dislocation nucleation mediated deformation and ultrahigh strength in sub-10-nm gold nanowires. Nano Res. 4, 1261–1267.
- Lu, Y., Sun, S., Zeng, Y., Deng, Q., Chen, Y., Li, Y., Li, X., Wang, L., Han, X., 2020. Atomistic mechanism of nucleation and growth of a face-centered orthogonal phase in small-sized single-crystalline Mo. Mater. Res. Lett. 8, 348–355.
- Luo, X.M., Li, X., Zhang, G.P., 2017. Forming incoherent twin boundaries: a new way for nanograin growth under cyclic loading. Mater. Res. Lett. 5, 95–101.
- Ma, E., 2020. Unusual dislocation behavior in high-entropy alloys. Scr. Mater. 181, 127–133.
- Misra, A., Hirth, J.P., Hoagland, R.G., 2005. Length-scale-dependent deformation mechanisms in incoherent metallic multilayered composites. Acta Mater. 53, 4817–4824.
- Naeem, M., He, H., Zhang, F., Huang, H., Harjo, S., Kawasaki, T., Wang, B., Lan, S., Wu, Z., Wang, F., 2020. Cooperative deformation in high-entropy alloys at ultralow temperatures. Sci. Adv. 6, eaax4002.
- Ogata, S., Li, J., Hirosaki, N., Shibutani, Y., Yip, S., 2004. Ideal shear strain of metals and ceramics. Phys. Rev. B 70, 104104.
- Oh, S.H., Legros, M., Kiener, D., Dehm, G., 2009. In situ observation of dislocation nucleation and escape in a submicrometre aluminium single crystal. Nat. Mater. 8,
- Park, H.S., Cai, W., Espinosa, H.D., Huang, H., 2009. Mechanics of crystalline nanowires. MRS Bull. 34, 178-183.
- Park, N.Y., Nam, H.S., Cha, P.R., Lee, S.C., 2015. Size-dependent transition of the deformation behavior of Au nanowires. Nano Res. 8, 941-947.
- Plimpton, S., 1995. Fast parallel algorithms for short-range molecular dynamics. J. Comput. Phys. 117, 1–19.
- Qin, Q., Yin, S., Cheng, G., Li, X., Chang, T.H., Richter, G., Zhu, Y., Gao, H., 2015. Recoverable plasticity in penta-twinned metallic nanowires governed by dislocation nucleation and retraction. Nat. Commun. 6, 1–8.
- Rabkin, E., Srolovitz, D.J., 2007. Onset of plasticity in gold nanopillar compression. Nano Lett. 7, 101-107.
- Ramachandramoorthy, R., Bernal, R., Espinosa, H.D., 2015a. Pushing the envelope of in situ transmission electron microscopy. ACS Nano 9, 4675-4685.
- Ramachandramoorthy, R., Gao, W., Bernal, R., Espinosa, H., 2015b. High strain rate tensile testing of silver nanowires: rate-dependent brittle-to-ductile transition. Nano Lett. 16, 255–263.
- Renk, O., Hohenwarter, A., Wurster, S., Pippan, R., 2014. Direct evidence for grain boundary motion as the dominant restoration mechanism in the steady-state regime of extremely cold-rolled copper. Acta Mater. 77, 401–410.
- Rogers, J.A., Someya, T., Huang, Y.G., 2010. Materials and mechanics for stretchable electronics. Science 327, 1603–1607.
- Rohith, P., Sainath, G., Choudhary, B., 2018. Effect of orientation and mode of loading on deformation behaviour of Cu nanowires. Comput. Condens. Matter. 17, e00330.
- Roos, B., Kapelle, B., Richter, G., Volkert, C., 2014. Surface dislocation nucleation controlled deformation of Au nanowires. Appl. Phys. Lett. 105, 201908.
- Sainath, G., Choudhary, B., Jayakumar, T., 2015. Molecular dynamics simulation studies on the size dependent tensile deformation and fracture behavior of body centered cubic iron nanowires. Comput. Mater. Sci. 104, 76–83.

- Sainath, G., Choudhary, B.K., 2016, Orientation dependent deformation behaviour of BCC iron nanowires, Comput. Mater. Sci. 111, 406-415.
- Schiøtz, J., Jacobsen, K.W., 2003. A maximum in the strength of nanocrystalline copper. Science 301, 1357-1359.
- Schneider, A.S., Kaufmann, D., Clark, B.G., Frick, C.P., Gruber, P.A., Monig, R., Kraft, O., Arzt, E., 2009. Correlation between critical temperature and strength of small-scale bcc pillars. Phys. Rev. Lett. 103, 105501.
- Schwaiger, R., Kraft, O., 1999. High cycle fatigue of thin silver films investigated by dynamic microbeam deflection. Scr. Mater. 41, 823-829.
- Sen, F.G., Alpas, A.T., Van Duin, A.C., Qi, Y., 2014. Oxidation-assisted ductility of aluminium nanowires. Nat. Commun. 5, 1-9.
- Seo, J.H., Park, H.S., Yoo, Y., Seong, T.Y., Li, J., Ahn, J.P., Kim, B., Choi, I.S., 2013. Origin of size dependency in coherent-twin-propagation-mediated tensile deformation of noble metal nanowires. Nano Lett. 13, 5112-5116.
- Seo, J.H., Yoo, Y., Park, N.Y., Yoon, S.W., Lee, H., Han, S., Lee, S.W., Seong, T.Y., Lee, S.C., Lee, K.B., 2011. Superplastic deformation of defect-free Au nanowires via coherent twin propagation. Nano Lett. 11, 3499-3502.
- Shan, Z., Mishra, R.K., Asif, S.S., Warren, O.L., Minor, A.M., 2008. Mechanical annealing and source-limited deformation in submicrometre-diameter Ni crystals. Nat. Mater, 7, 115.
- Shan, Z., Wiezorek, J.K., Stach, E., Follstaedt, D., Knapp, J., Mao, S., 2007. Dislocation dynamics in nanocrystalline nickel. Phys. Rev. Lett. 98, 095502.
- Shin, J., Chen, L.Y., Sanli, U.T., Richter, G., Labat, S., Richard, M.-I., Cornelius, T., Thomas, O., Gianola, D.S., 2019. Controlling dislocation nucleation-mediated plasticity in nanostructures via surface modification. Acta Mater. 166, 572-586.
- Stoppa, M., Chiolerio, A., 2014. Wearable electronics and smart textiles: a critical review. Sensors 14, 11957-11992. Basel.
- Stukowski, A., Albe, K., 2010. Extracting dislocations and non-dislocation crystal defects from atomistic simulation data. Model. Simul. Mater. Sci. Eng. 18, 085001. Sun, J., He, L., Lo, Y.C., Xu, T., Bi, H., Sun, L., Zhang, Z., Mao, S.X., Li, J., 2014a. Liquid-like pseudoelasticity of sub-10-nm crystalline silver particles. Nat. Mater. 13, 1007.
- Sun, J., He, L., Lo, Y.C., Xu, T., Bi, H., Sun, L., Zhang, Z., Mao, S.X., Li, J., 2014b. Liquid-like pseudoelasticity of sub-10-nm crystalline silver particles. Nat. Mater. 13, 1007-1012.
- Sun, S., Kong, D., Li, D., Liao, X., Liu, D., Mao, S., Zhang, Z., Wang, L., Han, X., 2019. Atomistic mechanism of stress-induced combined slip and diffusion in sub-5 nanometer-sized Ag nanowires. ACS Nano 13, 8708-8716.
- Tromans, D., 2011. Elastic anisotropy of HCP metal crystals and polycrystals. Int. J. Res. Rev. Appl. Sci. 6, 462-483.
- Van Swygenhoven, H., Derlet, P.M., Frøseth, A., 2004. Stacking fault energies and slip in nanocrystalline metals. Nat. Mater. 3, 399-403.
- Wang, J., Mao, S.X., 2016. Atomistic perspective on in situ nanomechanics. Extrem. Mech. Lett. 8, 127-139.
- Wang, J., Sansoz, F., Deng, C., Xu, G., Han, G., Mao, S.X., 2015a. Strong hall-petch type behavior in the elastic strain limit of nanotwinned gold nanowires. Nano Lett. 15, 3865-3870.
- Wang, J., Sansoz, F., Huang, J., Liu, Y., Sun, S., Zhang, Z., Mao, S.X., 2013a. Near-ideal theoretical strength in gold nanowires containing angstrom scale twins. Nat. Commun. 4, 1742.
- Wang, J., Sansoz, F., Huang, J., Liu, Y., Sun, S., Zhang, Z., Mao, S.X., 2013b. Near-ideal theoretical strength in gold nanowires containing angstrom scale twins. Nat. Commun. 4 (1), 1–8.
- Wang, J., Wang, Y., Cai, W., Li, J., Zhang, Z., Mao, S.X., 2018a. Discrete shear band plasticity through dislocation activities in body-centered cubic tungsten nanowires. Sci. Rep. 8 (1), 1-8.
- Wang, J., Zeng, Z., Weinberger, C.R., Zhang, Z., Zhu, T., Mao, S.X., 2015b. In situ atomic-scale observation of twinning-dominated deformation in nanoscale bodycentred cubic tungsten. Nat. Mater. 14, 594-600.
- Wang, J., Zeng, Z., Wen, M., Wang, Q., Chen, D., Zhang, Y., Wang, P., Wang, H., Zhang, Z., Mao, S.X., 2020a. Anti-twinning in nanoscale tungsten. Sci. Adv. 6, eaay2792.
- Wang, L., Kong, D., Zhang, Y., Xiao, L., Lu, Y., Chen, Z., Zhang, Z., Zou, J., Zhu, T., Han, X., 2017a. Mechanically driven grain boundary formation in nickel nanowires. ACS Nano 11, 12500-12508.
- Wang, L., Teng, J., Kong, D., Yu, G., Zou, J., Zhang, Z., Han, X., 2018b. In situ atomistic deformation mechanisms of twin-structured nanocrystal Pt. Scr. Mater. 147, 103_107
- Wang, L., Zhang, Z., Han, X., 2013c. In situ experimental mechanics of nanomaterials at the atomic scale. NPG Asia Mater. 5, e40 e40.
- Wang, L.H., Xin, T.J., Kong, D.L., Shu, X.Y., Chen, Y.H., Zhou, H., Teng, J., Zhang, Z., Zou, J., Han, X.D., 2017b. In situ observation of stress induced grain boundary migration in nanocrystalline gold. Scr. Mater. 134, 95–99.
- Wang, P., Chou, W., Nie, A., Huang, Y., Yao, H., Wang, H., 2011. Molecular dynamics simulation on deformation mechanisms in body-centered-cubic molybdenum nanowires. J. Appl. Phys. 110, 093521.
- Wang, P., Wu, Y., Liu, J., Wang, H., 2017c. Impacts of atomic scale lattice distortion on dislocation activity in high-entropy alloys. Extreme Mech. Lett. 17, 38-42. Wang, Q., Wang, J., Li, J., Zhang, Z., Mao, S.X., 2018c. Consecutive crystallographic reorientations and superplasticity in body-centered cubic niobium nanowires. Sci. Adv. 4 (7) eaas8850.
- Wang, S.J., Wang, H., Du, K., Zhang, W., Sui, M.L., Mao, S.X., 2014. Deformation-induced structural transition in body-centred cubic molybdenum. Nat. Commun. 5 (1), 1-9.
- Wang, X., Wang, J., He, Y., Wang, C., Zhong, L., Mao, S.X., 2020b. Unstable twin in body-centered cubic tungsten nanocrystals. Nat. Commun. 11, 1-7.
- Wang, X., Zhong, L., Mao, S., 2018d. Advances in understanding atomic-scale deformation of small-sized face-centered cubic metals with in situ transmission electron microscopy, Mater, Today Nano 2, 58-69.
- Wei, S., Wang, Q., Wei, H., Wang, J., 2019. Bending-induced deformation twinning in body-centered cubic tungsten nanowires. Mater. Res. Lett. 7, 210-216.
- Weinberger, C.R., Cai, W., 2008. Surface-controlled dislocation multiplication in metal micropillars. Proc. Natl. Acad. Sci. 105, 14304–14307.
- Weinberger, C.R., Cai, W., 2012. Plasticity of metal nanowires. J. Mater. Chem. 22, 3277-3292.
- Weinberger, C.R., Jennings, A.T., Kang, K., Greer, J.R., 2012. Atomistic simulations and continuum modeling of dislocation nucleation and strength in gold nanowires. J. Mech. Phys. Solids 60, 84-103.
- Wu, H.H., Trinkle, D.R., 2009. Cu/Ag EAM potential optimized for heteroepitaxial diffusion from ab initio data. Comput. Mater. Sci. 47, 577-583.
- Xu, F., Zhu, Y., 2012. Highly conductive and stretchable silver nanowire conductors. Adv. Mater. 24, 5117-5122.
- Yamakov, V., Wolf, D., Phillpot, S., Mukherjee, A., Gleiter, H., 2004. Deformation-mechanism map for nanocrystalline metals by molecular-dynamics simulation. Nat. Mater. 3, 43.
- Yan, J.W., Zhang, G.P., Zhu, X.F., Liu, H.S., Yan, C., 2013. Microstructures and strengthening mechanisms of Cu/Ni/W nanolayered composites. Philos. Mag. 93, 434-448.
- Yin, S., Cheng, G., Chang, T.H., Richter, G., Zhu, Y., Gao, H., 2019a. Hydrogen embrittlement in metallic nanowires. Nat. Commun. 10 (1), 1-9.
- Yin, S., Cheng, G., Richter, G., Gao, H., Zhu, Y., 2019b. Transition of deformation mechanisms in single-crystalline metallic nanowires. ACS Nano 13, 9082–9090.
- Yin, S., Cheng, G., Zhu, Y., Gao, H., 2020. Competition between shear localization and tensile detwinning in twinned nanowires. Phys. Rev. Mater. 4, 023603.
- Yue, Y., Zhang, Q., Zhang, X., Yang, Z., Yin, P., Guo, L., 2017. In situ observation of twin boundary sliding in single crystalline Cu nanowires. Small 13, 1604296. Zhang, J., Li, Y., Li, X., Zhai, Y., Zhang, Q., Ma, D., Mao, S., Deng, Q., Li, Z., Li, X., 2021. Timely and atomic-resolved high-temperature mechanical investigation of ductile fracture and atomistic mechanisms of tungsten. Nat. Commun. 12, 1-10.
- Zhang, Y., Chen, W., McDowell, D.L., Wang, Y.M., Zhu, T., 2020. Lattice strains and diffraction elastic constants of cubic polycrystals. J. Mech. Phys. Solids 138, 103899.
- Zhang, Z., Mao, M.M., Wang, J., Gludovatz, B., Zhang, Z., Mao, S.X., George, E.P., Yu, Q., Ritchie, R.O., 2015. Nanoscale origins of the damage tolerance of the highentropy alloy CrMnFeCoNi. Nat. Commun. 6 (1), 1-6.
- Zhang, Z., Sheng, H., Wang, Z., Gludovatz, B., Zhang, Z., George, E.P., Yu, O., Mao, S.X., Ritchie, R.O., 2017. Dislocation mechanisms and 3D twin architectures generate exceptional strength-ductility-toughness combination in CrCoNi medium-entropy alloy. Nat. Commun. 8 (1), 1-8.

- Zhao, S., Zhu, Q., An, X., Wei, H., Song, K., Mao, S.X., Wang, J., 2020a. *In situ* atomistic observation of the deformation mechanism of Au nanowires with twin-twin intersection. J. Mater. Sci. Technol. 53, 118–125.
- Zhao, S., Zhu, Q., Song, K., Zhou, H., Wang, J., 2020b. Role of intersecting grain boundary on the deformation of twin-twin intersection. Scr. Mater. 188, 184–189. Zheng, H., Cao, A., Weinberger, C.R., Huang, J.Y., Du, K., Wang, J., Ma, Y., Xia, Y., Mao, S.X., 2010. Discrete plasticity in sub-10-nm-sized gold crystals. Nat. Commun.
- Zheng, H., Wang, J., Huang, J.Y., Cao, A., Mao, S.X., 2012. *In Situ* visualization of birth and annihilation of grain boundaries in an Au nanocrystal. Phys. Rev. Lett. 109 (22), 225501.
- Zheng, S., Mao, S.X., 2021. Advances in experimental mechanics at atomic scale. Extreme Mech. Lett. 45, 101284.
- Zheng, S.X., Luo, X.M., Wang, D., Zhang, G.P., 2018. A novel evaluation strategy for fatigue reliability of flexible nanoscale films. Mater. Res. Express 5, 035012.
 Zheng, S.X., Luo, X.M., Zhang, G.P., 2020. Cumulative shear strain-induced preferential orientation during abnormal grain growth near fatigue crack tips of nanocrystalline Au films. J. Mater. Res. 1–8.
- Zhong, L., Sansoz, F., He, Y., Wang, C., Zhang, Z., Mao, S.X., 2017. Slip-activated surface creep with room-temperature super-elongation in metallic nanocrystals. Nat. Mater. 16, 439–445.
- Zhu, Q., Cao, G., Wang, J., Deng, C., Li, J., Zhang, Z., Mao, S.X., 2019. In situ atomistic observation of disconnection-mediated grain boundary migration. Nat. Commun. 10, 156.
- Zhu, T., Li, J., 2010. Ultra-strength materials. Prog. Mater. Sci. 55, 710-757.
- Zhu, T., Li, J., Samanta, A., Leach, A., Gall, K., 2008. Temperature and strain-rate dependence of surface dislocation nucleation. Phys. Rev. Lett. 100, 025502.
- Zhu, Y., 2017. Mechanics of crystalline nanowires: an experimental perspective. Appl. Mech. Rev. 69 (1).
- Zhu, Y., Liao, X., Wu, X., 2012. Deformation twinning in nanocrystalline materials. Prog. Mater. Sci. 57, 1–62.